SCIENCE CHINA
Technological Sciences

October 2012 Vol.55 No.10: 2960–2964
doi: 10.1007/s11431-012-4956-9

Effect of cooling rate on β→α transformation during quenching of a Zr-0.85Sn-0.4Nb-0.4Fe-0.1Cr-0.05Cu alloy

CHAI LinJiang[1], LUAN BaiFeng[1*], CHEN JianWei[1], ZHOU Jun[2] & LIU Qing[1]

[1] *College of Materials Science and Engineering, Chongqing University, Chongqing 400044, China;*
[2] *Northwest Institute for Non-ferrous Metal Research, Xi'an 721014, China*

Received March 1, 2012; accepted May 7, 2012; published online June 23, 2012

The effect of β→α cooling rate during quenching on a new Zr-Sn-Nb-Fe-Cr-Cu alloy is reported. The microstructure evolution is well characterized by electron channeling contrast (ECC) imaging and transmission electron microscopy (TEM) techniques. The results show that specimens cooled by water, liquid nitrogen, air and furnace from β-phase present martensitic, coarse basket-weave, parallel-plate and lenticular structure, respectively. Residual β phase is detected by performing electron diffraction and composition analysis in the furnace cooled specimen. Micro hardness values of specimens decrease while the width of α laths increase with the cooling rate decreasing. The preliminarily established quantitative relationship among the cooling rate, microstructure and mechanical properties will shed light on the microstructure control and property optimization.

zirconium alloy, microstructure, cooling rate, phase transformation, hardness

Citation: Chai L J, Luan B F, Chen J W, et al. Effect of cooling rate on β→α transformation during quenching of a Zr-0.85Sn-0.4Nb-0.4Fe-0.1Cr-0.05Cu alloy. Sci China Tech Sci, 2012, 55: 2960–2964, doi: 10.1007/s11431-012-4956-9

1 Introduction

Among the new zirconium alloys developed for water-cooled nuclear reactors in recent years, a low Nb containing alloy series in which N18 (Zr-1Sn-0.3Nb-0.3Fe-0.1Cr) acts as a representative is a group of promising cladding materials [1, 2]. For the new alloy system, optimum manufacturing processes are significant factors to improve properties and need urgently to be established. During conventional fabrications, fuel cladding materials are often heated into β phase temperature ranges and then cooled to room temperature to produce controlled precipitation during the subsequent aging. Further, in recent years β-quenching at the final stage in the fabrication process of zirconium alloys has been regarded as an important process for advanced fuel cladding materials [3–5].

It is well known that zirconium alloy will transform from a β body-centred cubic (bcc) phase to an α hexagonal close-packed (hcp) phase during β quenching. But the α phase can get different microstructures when treated at different cooling conditions. For Zircaloys, lenticular, parallel-plate, basket-weave, martensitic structures have been reported when cooled at the rates covering less than one to thousands of Celsius degrees per second [5–14]. For new Nb-containing zirconium alloys, however, only the martensitic structure obtained by quenching in water has been tentatively characterized in Zirlo [15], HANA-6 [16] and Zr-xNb binary alloys [15, 17, 18]. Currently, there is no systematic study on the other three sorts of structures or on the effect of cooling rate on them. Generally, these quenched structures are mainly studied by conventional transmission electron microscopy (TEM) for characterizing micro-twins, dislocations and fine precipitates, and optical microscopy (OM) for

*Corresponding author (email: bfluan@cqu.edu.cn)

observing macro morphologies of α phases. Problems could emerge as the morphology of needle-shaped grains of martensitic structures cannot be clearly observed due to the limited resolution of OM [6–8]. On the other hand, the TEM is not so adequate in identifying the coarse-grain lenticular structure because of the very limited vision field at unavoidably high magnification [13]. Fortunately, an imaging method based on electron channeling contrast (ECC) technique which can make up the discrepancy between TEM and OM has been successfully applied in recent years [19–21], yet not very much in zirconium alloy [22]. The ECC technique may be a powerful tool to characterize the quenched microstructure since its signals are extremely sensitive to crystallographic orientations. In addition, the quantitative relationship between β cooling rate and the α phase structure in zirconium alloys has not been well documented to date. However, the establishment of this relationship can facilitate the precise microstructure control, which can lay a good foundation for property optimization.

Therefore, this work employs mainly the ECC technique in characterizing the microstructure evolution with different β-cooling rates for a Zr-0.85Sn-0.4Nb-0.4Fe-0.1Cr-0.05Cu alloy. Also, with the help of ECC images and hardness tests, we have attempted to preliminarily realize the quantitative characterization of the relationship among cooling rate, microstructure and hardness of specimens.

2 Experimental

The as-received Zr-0.85Sn-0.4Nb-0.4Fe-0.1Cr-0.05Cu alloy plates with a thickness of 1.4 mm supplied by Northwest Institute for Non-ferrous Metal Research (NINMR) possessed an initial state of fully recrystallized. Specimens with dimensions of 8 mm × 6 mm cut from the as-received plate were cooled in various cooling processes from the β-region of 1030°C for 40 min, such as water cooling (W.C), liquid nitrogen cooling (LN.C), air cooling (A.C) and furnace cooling (F.C). The cooling rates of various cooling processes were about 1000, 100, 5 and 0.05°C/s, respectively, according to refs. [4, 13, 16]. A special attention should be paid to the cooling rate value of LN.C, which was believed to be similar to the more frequently selected oil cooling condition.

The specimens with different β cooling rates were mainly characterized by a scanning electron microscopy (SEM, FEI NOVA 400) equipped with a back scattering electron (BSE) detector. In this investigation, the BSE detector was used to produce ECC images. As a supplement, transmission electron microscope (TEM, LIBRA 200) was selected to investigate the microstructure that the ECC images cannot discriminate. Precipitates were analyzed by use of both energy dispersive spectroscopy (EDS) and selected area diffraction (SAD) in TEM. The widths of α laths were acquired using an image analyzer and the hardness of the samples was measured by a Vickers indentation (EVERONE MH-5L) at a 490MN load. For the hardness determination, an average value of 10 measurements was taken for each sample.

3 Results and discussion

The macroscopic microstructures of all specimens are shown in Figure 1. The specimen cooled into water from β-phase exhibits the fine-needle structure (Figure 1(a)). But it is difficult to identify whether the needle-shape structure is martensite or not under such a low magnification. When the cooling rate is slowed down to about 100°C/s as in the case of liquid nitrogen cooling, the α needles get coarser (Figure 1(b)). And the overall structure represents a typical basket-weave Widmanstätten with an appearance of short plates intersecting each other. After air cooling (at a rate of about 5°C/s), there exists a parallel-plate Widmanstätten with long plates growing from the parent β-grain boundaries (Figure 1(c)). In case of the furnace cooling of which the cooling rate is as low as about 0.05°C/s, the coarser grains totally different from the Widmanstätten structure are observed (Figure 1(d)).

To further investigate the detailed microstructure, high-magnification SEM-ECC images which can reveal α-lath shape, size and precipitate distribution were acquired as in Figure 2, which clearly shows the α-lath microstructure of the water cooling specimen without visible precipitates in the matrix. It was also found that there were three main growth orientations for those α laths and it is 60° between any two of the growth orientations as have been marked in Figure 2(a). Typical Widmanstätten of the basket-weave and parallel-plate structures with fine precipitates decorat-

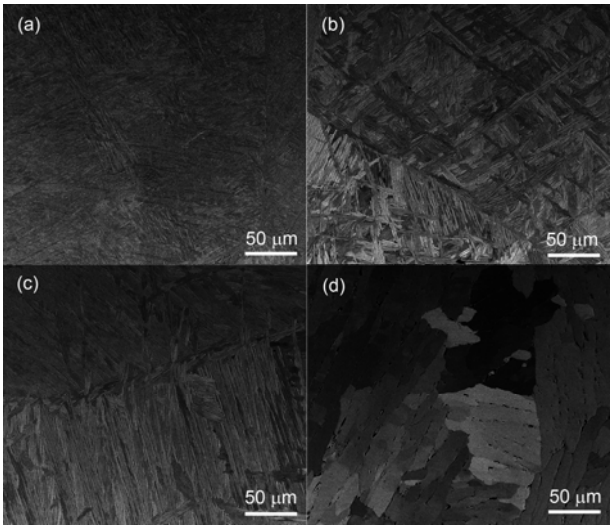

Figure 1 SEM-ECC images of macroscopic microstructures of the Zr-0.85Sn-0.4Nb-0.4Fe-0.1Cr-0.05Cu alloy cooled by various cooling processes: (a) Water cooling; (b) liquid nitrogen cooling; (c) air cooling; (d) furnace cooling.

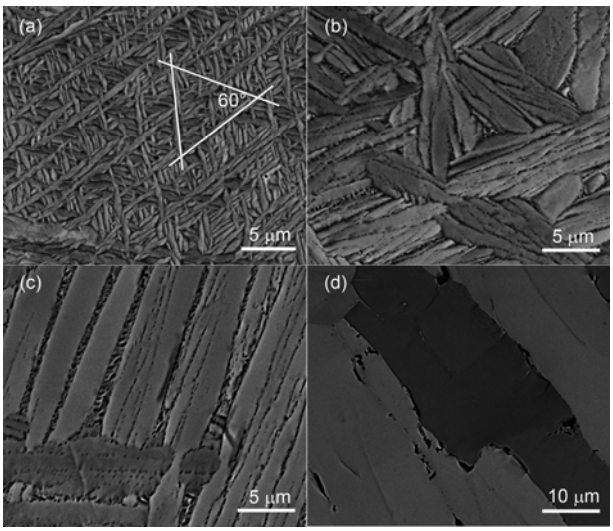

Figure 2 SEM-ECC microstructure images of the Zr-0.85Sn-0.4Nb-0.4Fe-0.1Cr-0.05Cu alloy cooled by various cooling processes: (a) Water cooling; (b) liquid nitrogen cooling; (c) air cooling; (d) furnace cooling.

ing the lath boundaries are presented in Figures 2(b) and (c), respectively. Moreover, the furnace cooling specimen with the slowest cooling rate exhibits larger and net-like precipitates distributed along grain boundaries (Figure 2(d)).

Perez et al. [9] reported that an α phase microstructure was martensite only for cooling rate exceeding 1500°C/s in Zircaloy-4. However, when comparing the compositions of Zircaloy-4 and the alloy used in this work, it is found that the later one contains more β-stabilizer elements (Nb, Fe and Cu) and less α-stabilizer elements (Sn). Woo et al. [8] concluded that the decreased amount of α-stabilizer such as O elements would make the critical cooling rate for martensitic phase transformation decrease. So it might be reasonable to deduce that the water cooling rate (about 1000°C/s) in this study is fast enough to induce martensitic transformation for the Zr-0.85Sn-0.4Nb-0.4Fe-0.1Cr-0.05Cu alloy. Besides, the good orientation relationship among α laths (Figure 2(a)) and absence of precipitates in W.C specimen can be thought to be strong direct evidences of the diffussionless martensitic transformation as has been figured out by Kim et al. [16] and Neogy et al. [15]. Furthermore, Figure 3(a) shows a high-magnification TEM image of the W.C specimen which owns a higher spatial resolution than ECC images. Although the sample preparation method differs largely with the ECC and the resolution is improved enough to discriminate nano-scale particles, the result is almost the same, that is, no precipitate exists in matrix after water cooling. This provides a more solid evidence of the diffusion-less martensitic transformation and also confirms the validation of the above ECC results.

In specimens quenched at relatively slow rates such as at the conditions of the liquid nitrogen cooling and air cooling, the β to α transformation presumably involves nucleation and growth of the α phase by a diffusion process. It was proposed [7] that at the initial stage of β phase cooling, for the basket-weave structure, there are an abundant α phase nucleation sites inside the β grains. Those α plate nuclei grow on many habit planes owing to the cubic symmetry of the β phase but will be interrupted by other α plates before growing very long, while for parallel-plate structure, because of the absence of those nucleation sites, α plates start growing from grain boundaries. With respect to the specific

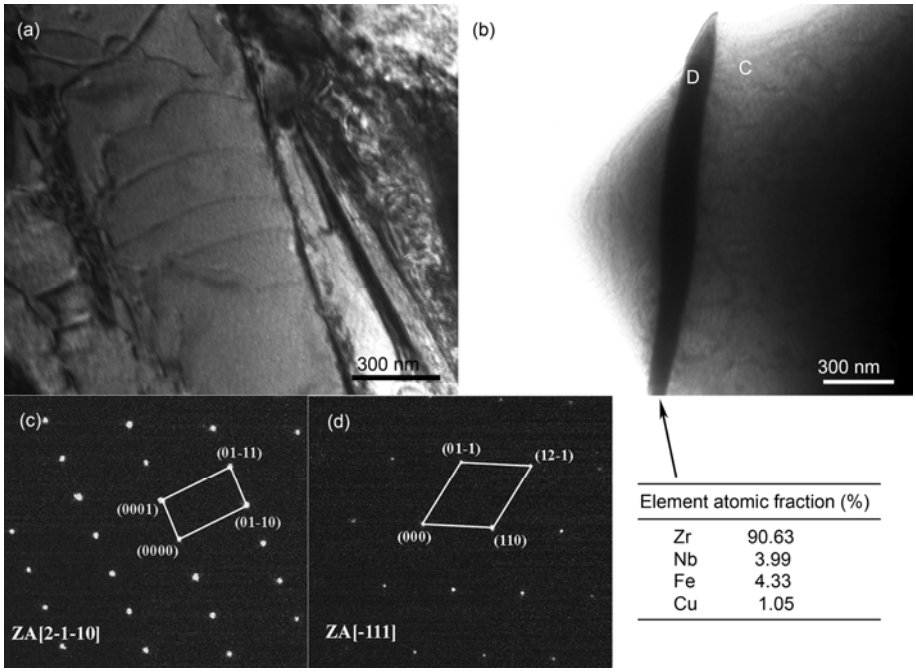

Figure 3 TEM bright field images of (a) water cooling and (b) furnace cooling specimens. (c) and (d) are selected area diffraction patterns corresponding to C and D points in (b), respectively.

orientation of any prior β grain, a single habit plane will probably be favorable and then a cluster of parallel plates grows into the β grain. During further cooling these plates thicken laterally. At the same time, diffusion processes help transport as many solutes (viz., Nb, Fe, Cr, Cu) as possible into the untransformed β phase inter α laths. The combination of the above processes finally results in the mcirostructures indicated by Figures 2(b) and (c).

Figure 3(b) shows a TEM bright field image of the F.C specimen and a micro chemical analysis result of the net-like inter-lath precipitate. Alloying elements Nb, Cu and Fe are frequently detected in those inter-lath precipitates. Furthermore, the TEM-SAD patterns in Figures 3(c) and (d) clearly reveal that the net-like inter-lath phase corresponds to β-Zr (JCPDF #34-0657, a=0.355 nm). In Nb-containing Zr alloys, residual β-Zr is frequently reported when cooled form high temperature [23], which is consistent with the present results.

By comparing the microstructure with different β cooling rates in zirconium alloy, it has been figured out that the α-lath width could be seen as a characteristic parameter [8]. Therefore, by measuring the widths of α laths that present in ECC images with proper magnifications, we can further investigated the effect of cooling rates on microstructure evolution in the aspect of quantitative analysis. The width of α laths as a function of the cooling rate is shown in Figure 4, which indicates that the width of the laths decreases with an increase of cooling rate. Moreover, there is almost a linear relationship between logarithmic value of α-lath width and cooling rate. This relationship is found to be in a good agreement with the theoretical analysis result of refs. [5, 14, 24], in which Massih et al. presented the findings of their work in detail.

Figure 4 also gives a varying trend of the micro Vickers hardness with cooling rate for the Zr-0.85Sn-0.4Nb-0.4Fe-0.1Cr-0.05Cu alloy. It can be seen that the increasing cooling rate generally corresponds to a higher hardness, which is consistent with previous results of Zircaloy-4 [11]. It is well known that the hardening of metallic materials is associated with several factors such as solid solution, precipitates and grain boundaries, all of which are involved in the present investigation. In the W.C specimen, almost all solute atoms are supersaturated in matrix and the finest α lath (0.5 μm) proves it possess the densest grain boundaries in all the specimens investigated. These factors co-produce a maximum hardness of 233 HV. Whereas for the LN.C specimen, a lower hardness of 212 HV was obtained, though many precipitates were observed inter laths which may contribute to a precipitation hardening effect. In fact, the LN.C specimen owns coarser α lath (1 μm) that will weaken the grain boundary hardening effect. Therefore, it seems that the boundary hardening predominates the contribution to the hardness as compared to other factors. This deduction is validated by the fact that the A.C and F.C specimens which

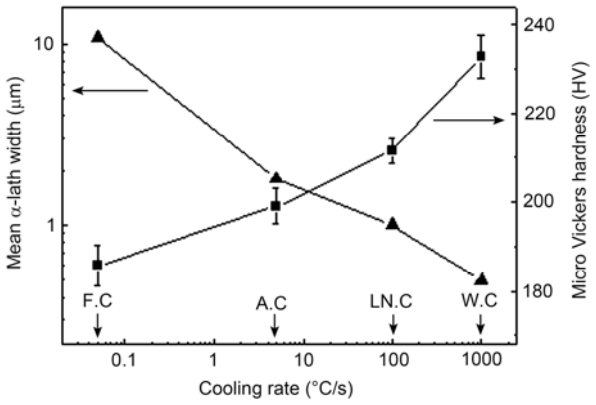

Figure 4 Mean α-lath width and micro Vickers hardness varying with cooling rate in the Zr-0.85Sn-0.4Nb-0.4Fe-0.1Cr-0.05Cu alloy.

own larger widths (2 μm and 11 μm, respectively) of α laths show further lower hardness 199 HV and 186 HV, respectively.

Therefore, with the aid of a specific parameter of "mean α-lath width", the relationship of α phase microstructure and β cooling rate is clearly revealed. Meanwhile, it can also be seen that the hardness value can adequately reflect its microstructural characteristic. Considering the industrial application of β cooling process, this work demonstrates that by simply taking hardness tests, it is possible to realize process control thus optimize it.

4 Conclusion

This work reports the effect of cooling rate on β→α transformation during quenching of a Zr-0.85Sn-0.4Nb-0.4Fe-0.1Cr-0.05Cu alloy. The acquired high-quality ECC images demonstrate that specimens cooled by water, liquid nitrogen, air and furnace from β-phase present martensitic, coarse basket-weave, parallel-plate and lenticular structure in sequence. There is an experimentally linear-decreasing relationship between logarithmic value of α-lath width and cooling rate and this is consistent with theoretical results. The micro hardness test result reveals that by increasing cooling rate, micro hardness increases accordingly. The preliminary establishment of quantitative relationships among cooling rate, microstructure and hardness could facilitate the microstructure and process control to realize property optimization.

The authors would like to thank Dr. Y H JEONG of KAERI for useful comments. Dr. N KAWUNGA is also gratefully acknowledged for the language revising work of this manuscript. This work was supported by the programs of New Century Excellent Talents in University (Grant No. NCET-08-0606), the Sharing Fund of Chongqing University's Large-scale Equipment, and the Fundamental Research Funds for the Central Universities of China (Grant Nos. CDJZR10130008 and CDJXS10132201).

1 Liu W Q, Li Q, Zhou B X, et al. Effect of heat treatment on the microstructure and corrosion resistance of a Zr-Sn-Nb-Fe-Cr alloy. J Nucl Mater, 2005, 341: 97–102
2 Zhang H X, Fruchart D, Hlil E K, et al. Crystal structure, corrosion kinetics of new zirconium alloys and residual stress analysis of oxide films. J Nucl Mater, 2010, 396: 65–70
3 Dahlbäck M, Limbäck M, Hallstadius L, et al. The effect of beta-quenching in final dimension on the irradiation growth of tubes and channels. In: 14th International Symposium on Zirconium in the Nuclear Industry, ASTM STP 1467, West Conshohocken, 2005. 276–304
4 Hong H S, Kim S J, Lee K S. Effect of oxygen content on the beta-quenched microstructure of modified Zircaloy-4. J Nucl Mater, 1999, 265: 108–111
5 Massih A R, Dahlbäck M, Limbäck M, et al. Effect of beta-to-alpha phase transition rate on corrosion behavior of Zircaloy. Corros Sci, 2006, 48: 1154–1181
6 Holt R A. The beta to alpha phase transformation in Zircaloy-4. J Nucl Mater, 1970, 35: 322–334
7 Ökvist G, Källström K. The effect of zirconium carbide on the beta to alpha transformation structure in Zircaloy. J Nucl Mater, 1970, 35: 316–321
8 Woo O T, Tangri K. Transformation characteristics of rapidly heated and quenched Zircaloy-4-oxygen alloys. J Nucl Mater, 1979, 79: 83–94
9 Perez T E, Saggese M E. Welding structures in gas tungsten arc-welded Zircaloy-4. Metallography, 1982, 15: 43–52
10 Quach V, Northwood D O. Influence of the phosphorus impurity content on the microstructure of Zircaloy-4 air cooled from the high temperature beta phase region. Metallography, 1984, 17: 191–201
11 Jeong Y H, Kim U C. Correlation of cold work, annealing and microstructure in Zircaloy-4 cladding material, J Korean Nucl Soc, 1986, 18: 267–272
12 Charquet D, Alheritiere E. Influence of impurities and temperature on the microstructure of Zircaloy-2 and Zircaloy-4 after the beta-alpha phase transformation. In: 7th International Symposium on Zirconium in the Nuclear Industry, ASTM STP 939, Philadelphia, A, 1987. 284–291
13 Jeong Y H, Rheem K S, Choi C S, et al. Effect of beta heat treatment on microstructure and nodular corrosion of Zircaloy-4. J Nucl Sci Technol, 1993, 30: 154–163
14 Massih A R, Andersson T, Witt P, et al. Effect of quenching rate on the beta to alpha phase transformation structure in zirconium alloy. J Nucl Mater, 2003, 322: 138–151
15 Neogy S, Srivastava D, Chakravartty J, et al. Microstructural evolution in Zr-1Nb and Zr-1Nb-1Sn-0.1 Fe alloys. Metall Mater Trans A, 2007, 38: 485–498
16 Kim H G, Baek J H, Kim S D, et al. Microstructure and corrosion characteristics of Zr-1.5Nb-0.4Sn-0.2Fe-0.1Cr alloy with a beta-annealing. J Nucl Mater, 2008, 372: 304–311
17 Srivastava D, Mukhopadhyay P, Banerjee S, et al. Morphology and substructure of lath martensites in dilute Zr-Nb alloys. Mat Sci Eng A, 2000, 288, 101–110
18 Jeong Y H, Lee K O, Kim H G. Correlation between microstructure and corrosion behavior of Zr-Nb binary alloy. J Nucl Mater, 2002, 302: 9–19
19 Huang C X, Wang K, Wu S D, et al. Deformation twinning in polycrystalline copper at room temperature and low strain rate. Acta Mater, 2006, 54: 655–665
20 Li Y S, Zhang Y, Tao NR, et al. Effect of thermal annealing on mechanical properties of a nanostructured copper prepared by means of dynamic plastic deformation. Scripta Mater, 2008, 59: 475–478
21 Guo N, Liu Q, Xin Y C, et al. The application of back-scattered electron imaging for characterization of pearlitic steels. Sci China Tech Sci, 2011, 54: 2368–2372
22 Luan B F, Chai L J, Chen J W, et al. Growth behavior study of second phase particles in a Zr-Sn-Nb-Fe-Cr-Cu alloy. J Nucl Mater, 2012, 423: 127–131
23 Zhou B X, Yao M Y, Li Q, et al. Nodular corrosion resistance of Zr-Sn-Nb alloy. Rare Metal Mat Eng, 2007, 36: 1317–1321
24 Massih A R, Jernkvist L O. Phase ordering under quenching: a case of Zr-alloy. J Phys Chem Solids, 2004, 65:1193–1198